Signal, Image and Video Processing (2023) 17:1035–1041
https://doi.org/10.1007/s11760-022-02309-w

ORIGINAL PAPER

Deep convolutional neural networks for detection of abnormalities in chest X-rays trained on the very large dataset

Kadir Aktas[1,2] · Vuk Ignjatovic[3] · Dragan Ilic[3] · Marina Marjanovic[3] · Gholamreza Anbarjafari[1,2,4,5]

Received: 31 August 2021 / Revised: 10 April 2022 / Accepted: 28 June 2022 / Published online: 20 July 2022

Abstract

One of the main challenges in the current pandemic is the detection of coronavirus. Conventional techniques (PT-PCR) have their limitations such as long response time and limited accessibility. On the other hand, X-ray machines are widely available and they are already digitized in the health systems. Thus, their usage is faster and more available. Therefore, in this research, we evaluate how well deep CNNs do when it comes to classifying normal versus pathological chest X-rays. Compared to the previous research, we trained our network on the largest number of images, 103,468 in total, including 5 classes such as COPD signs, COVID, normal, others and Pneumonia. We achieved COVID accuracy of 97% and overall accuracy of 81%. Additionally, we achieved classification accuracy of 84% for categorization into normal (78%) and abnormal (88%).

Keywords Optimization of convolutional neural network · Automatic diagnosis of COVID-19 · X-ray · Swarm intelligence

1 Introduction

The most talked-about current pandemic, COVID-19, has resulted in a massive global tragedy and has had a significant influence on many lives throughout the world. The first case of the fatal virus was reported in Wuhan, a Chinese province in December 2019 [1]. The virus swiftly spread throughout the world, affecting a wide range of countries.

One of the most frequently used techniques for diagnosing COVID-19 is reverse transcription-polymerase chain reaction (RT-PCR). Early identification of the disease has relied heavily on radiological imaging techniques such as computed tomography (CT) and X-ray [2]. X-ray scans have been utilized in the screening of COVID-19 patients since PCR has a diagnostic sensitivity of 60%-70%. In a few recent studies, it is observed that X-ray and CT imaging scans of people who have COVID-19 symptoms are altered [3]. Zhao et al. [4] found dilatation and consolidation in COVID-19 patients, as well as ground-glass opacities.

The rapid rise in positive COVID-19 cases has increased the need for researchers to employ Artificial Intelligence (AI) in conjunction with the expert opinion to assist clinicians in their jobs. In this regard, deep learning models have begun to gain momentum. Because radiologists are in short supply in hospitals, AI-based diagnostic models might be beneficial in giving prompt assistance to patients. Hemdan et al. [5] proposed seven Convolutional Neural Network (CNN) models to diagnose COVID-19 from X-ray images, including improved VGG19 and Google MobileNet. With an accuracy of 92.4%, Wang et al. [6] identified COVID-19 images from normal and viral pneumonia patients. Similarly, Ioannis et al. [7] used 224 COVID-19 images and achieved

This work has been partially supported by the Estonian Centre of Excellence in IT (EXCITE) funded by the European Regional Development Fund. We gratefully acknowledge the support of NVIDIA Corporation with the donation of the Titan Xp GPU used for this research.

✉ Kadir Aktas
kadir.aktas@ut.ee

Vuk Ignjatovic
vuk.ignjatovic.18@singimail.rs

Dragan Ilic
dragan.ilic.17@singimail.rs

Marina Marjanovic
mmarjanovic@singidunum.ac.rs

Gholamreza Anbarjafari
shb@ut.ee

1 iCV Research Lab, Institute of Technology, University of Tartu, 51009 Tartu, Estonia

2 iVCV OÜ, 51011 Tartu, Estonia

3 Singidunum University, Belgrade 11010, Serbia

4 PwC Advisory, Helsinki, Finland

5 Yildiz Technical University, Istanbul, Turkey

a class accuracy of 93.4%. Opconet, an optimized CNN, was suggested in [8] with a total of 2800 images and a 92.8% accuracy score. Apostolopoulous et al. [9] created a MobileNet CNN model utilizing extricated features. Various other methods, such as InceptionV3, ResNet50, GCN, and Inception-ResNetV2, were used for classification [10–13]. In [14], a transfer learning-based method was employed in order to classify existence or absence of COVID-19 chest X-ray pictures utilizing three models such as ResNet18, ResNet50, SqueezeNet, and DenseNet121. In [15], CNN's key hyperparameters are tuned using (i) MLP and Grey Wolf Optimizer (GWO), and (ii) MLP and Whale optimization + BAT method.

Although all of the above-mentioned state-of-the-art approaches use CNN, the methods do not take into consideration more than 6432 images. Using such a small dataset causes many real life cases to be missed out. Data augmentation can be performed to overcome this issue. But, in this case, data augmentation techniques such as rotation and resizing of the pictures are not enough to cover wide range of possible cases for COVID-19 instances, viral pneumonia, and normal chest X-ray scans. As a result, the generated CNN models fail to properly distinguish these diseases. Although some degree of inaccuracy in recognizing viral pneumonia cases is acceptable, misclassification of COVID-19 patients as normal or viral pneumonia might confuse physicians and management. The proposed study attempts to solve the constraints described above by creating an automated diagnostic method for screening COVID-19 patients using chest X-ray images trained on 103,468 images considering 5 classes such as COPD signs, COVID, normal, others and Pneumonia.

The remaining part of this paper is structured as follows: Section 2 explains the dataset in details. Section 3 introduces the proposed method. Section 4 presents the experimental results. Finally, Sect. 5 concludes the paper.

2 Dataset description

Four distinct datasets make up our data collection. We combined the following datasets PADCHEST dataset [16], BIMCV-COVID19+ dataset [17], COVID-19 Radiography Database ([18] and [19]), and Chest X-ray Images (Pneumonia) [20]. We employ 297,541 frontal chest X-ray images from 86,876 individuals by merging all the datasets. We did not apply a processing technique on the images while collecting the dataset. There are an average of 3-4 images per subject due to the follow-up scans. As a result, for all studies, patient-wise splits are taken into account to divide the patients into training, validation, and test groups. Some anomaly classes provide geographical information in the PLCO dataset. Table 1 depicts the number of images that each anomaly was found in. Multiple anomalies can be seen in a single picture. Furthermore, the collections comprise 178,319 images that do not exhibit any of the previously described anomalies; these images are not listed in Table 1.

Table 1 Number of images for each anomaly in the dataset

Class	Number of samples
Normal	62,115
Pulmonary fibrosis	760
Heart insufficiency	1722
COPD signs	23,280
Pneumonia	7747
Tuberculosis sequelae	399
Emphysema	734
Pulmonary artery hypertension	8
Tuberculosis	152
Atypical pneumonia	234
Bone metastasis	150
Lung metastasis	326
Pulmonary oedema	458
Asbestosis signs	69
Pulmonary hypertension	148
Post radiotherapy changes	138
Respiratory distress	35
Lymphangitis carcinomatosa	21
Lepidic adenocarcinoma	11
Covid	3616
Viral pneumonia	1345

We used a total of 103,476 images in our experiments. As it can be seen in Table 1, there is a huge bias between the classes. For example "normal" and "COPD signs" have 62,115 and 23,280 samples, respectively, while many other classes have less than 1,000 samples each. In order to prevent this dataset bias, we grouped up similar classes under the same label and proceeded on the experiments with the newly assigned labels. Also, we excluded 136 images that have broken file format hence creating problems for us while reading the file.

Given D1 = 14 abnormalities of the ChestX-ray14 dataset and D2 = 12 abnormalities of the PLCO dataset, we define D = D1 + D2 = 26 classes for our network. In our first set of experiments, we splitted the dataset into 5 classes (See Table 2). Since "normal", "COPD signs", "pneumonia", and "covid" has plenty of samples, we kept them as they are. On the other hand, we combined all the smaller classes under one label called "others".

In our second set of experiments, we splitted the dataset into 2 classes (See Table 3). We kept "normal" class as it is, and combined all other classes under "abnormal" label where "normal" indicates image of a healthy lung, and "abnormal" indicates an unhealthy lung.

Table 2 Dataset splitted into 5 labels

Class	Number of samples
Normal	62,108
COPD signs	23,277
Pneumonia	9092
Covid	3616
Others	5239

Table 3 Dataset splitted into 2 labels

Class	Number of samples
Normal	62,108
Abnormal	40,132

3 Proposed method

3.1 Network

In our method, we firstly extract the most important features of the images that are distinguishing between the classes. Then, we use a classifier to obtain the results. Considering X-ray scans of lungs, distinguishing features can be obtained from the texture. For example, X-ray scan of a lung with pneumonia has abnormalities in the texture compared to a normal, i.e. healthy lung (See Table 4). Our aim is to catch such features to find patterns for each class.

The state-of-the-art research show that one of the most successful ways of obtaining texture features from the images is using CNN-based deep learning methods [15,21–23]. Thanks to their convolutional structure, these methods process each pixel and their relation with neighbouring pixels together. This way, they successfully find the features in the images. Therefore, we used a CNN-based network as our feature extractor.

In our method, we pass the processed images to a InceptionV3 network which we use as our boneback for feature extraction. In order to pick the best boneback network here, we experimented with different boneback networks and picked InceptionV3 since it performs the best in our case. Discussion on these experiment can be found in the results section. InceptionV3 is a convolutional neural network-based architecture which is made of symmetric and asymmetric blocks. As it can be seen in Fig. 1, the network has a deep architecture in which the convolution layers create the base, and fully connected layers are used to make a connection to output. Average pooling, max pooling, batch normalization and dropouts are also used in the network to improve the performance.

Lastly, we use a classifier to obtain the final label using the features extracted. In our classifier, firstly, we pass the features through a normalization layer. This is done to regularize the data. We use batch normalization which processes the data batch by batch and subtracts mean, and divides by standard deviation [25]. After that, two fully connected layers with sizes of 64 and 32 are added to model the relationship between the extracted features and the final classes. We used ReLu activation in these layers. Additionally, we included dropout layers with 0.5 rate after each fully connected layer to prevent overfit. Finally, an output layer is included to obtain the final prediction per class.

3.2 Training

The training has been carried out with a batch size of 128. We used 20 epochs as this epoch number is enough for converging in our case. Higher epoch numbers are resulted with overfitting. 5 folds cross-validation is applied to avoid a biased data split. Larger fold numbers are not preferred as it increases the training time a lot.

For all of our experiments, we splitted the dataset into training and testing sets with a ratio of 0.75 and 0.25, respectively. Only the training set is used for training and validation while testing set is used only for the testing after the training process is completed.

Table 4 Samples from the dataset

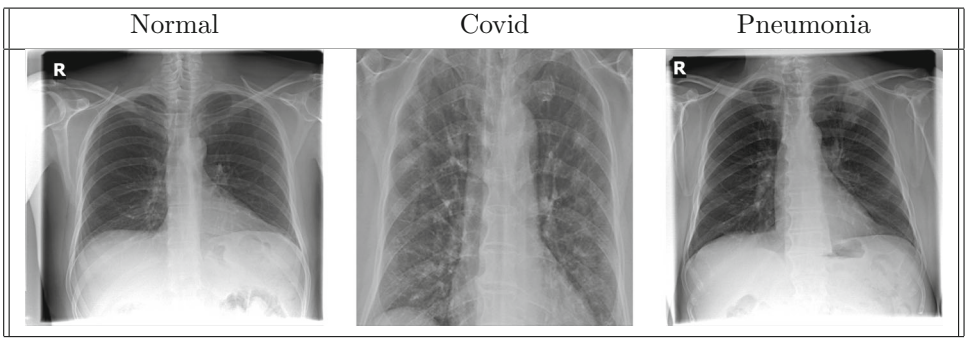

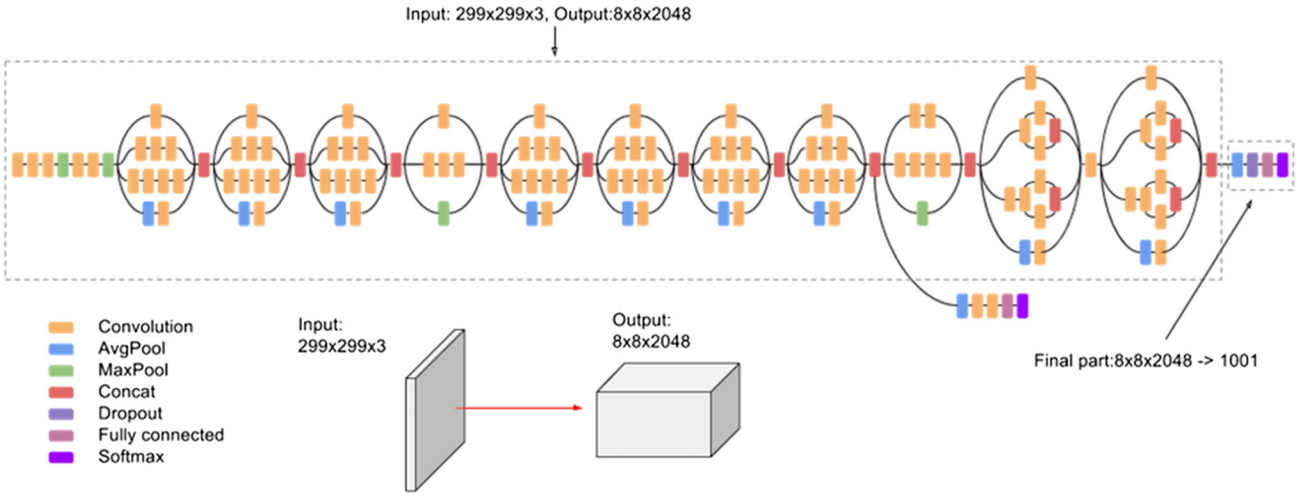

Fig. 1 InceptionV3 architecture [24]

Table 5 Results for each backbone for 2-class and 5-class

Backbone	2-class (%)	5-class (%)
VGG16	83.84	79.14
InceptionV3	84.57	81.03
ResNet50	83.08	74.61
NasNetMobile	73.41	68.13

Table 6 Class accuracies when InceptionV3 is used as backbone

2-class accuracies	Normal 78.33%
	Abnormal 88.60%
5-Class accuracies	COPD signs 62.93%
	Covid 97.03%
	Normal 93.20%
	Pneumonia 64.46%
	Others 34.25%

All the experiments are done on a PC with Ubuntu 20.04 installed. Main hardware used are Intel®Core™ i7-5820K central processing unit, NVIDIA TITAN Xp graphics processing unit and 96 gigabytes of memory.

4 Results

In this task, X-ray images are very similar to each other, resulting with a low inter-class variance in the dataset. Therefore, extracting the distinctive features is important to have a good performing method. In our experiments, we focused on this idea to improve the performance. We conducted experiments with different feature extraction backbones to evaluate their contributions to the overall performance. As explained in Sect. 3 in details, we selected the most commonly used state-of-the-art CNN-based networks, i.e. VGG16 [26], InceptionV3 [24], ResNet50 [27], NasNetMobile [28], for this experiment. We conducted the same experiment for both 5-class and 2-class dataset label grouping.

In Table 5, you can see how well our method performs when different backbones are used. We measured the performances on the test split for both 2-class and 5-class splits. From the table, we can see that performances of all the backbones are better for 2-class merge compared to 5-class merge. This is an expected result for us as 2-class split in this task is created between normal and abnormal (diseased) X-ray images. Variance between the diseased and normal images is higher than the variance in 5-class dataset. In 5-class merge, the network needs to characterize and separate four pathological classes from each other. However, this is a hard task as these classes have a low variance among each other. Secondly, 'others" class in 5-class merge has a low accuracy, resulting with a decrease in the overall accuracy. Looking at the accuracies in the table, we can see that VGG16, InceptionV3 and, ResNet50 perform very close to each other for 2-class. However, their performances differ for 5-class as InceptionV3 leads with 81.03% test accuracy.

In order to elaborate on the performance more, we present the class accuracies of our method using InceptionV3 backbone for 2-class and 5-class splits in Table 6. We discuss that the main difference between class accuracies is caused by the low variance and difference in the sample counts between them. Also, it is notable that in Table 6, "others" class has a very low accuracy. As explained in Sect. 2, we merged many classes which have a low sample count to create "others" class. Therefore, this class both have a low sample count and a hard-to-characterize sample set. We argue that these two factors are the main reasons behind the low accuracy for "others" class. Furthermore, we calculated Matthews Correlation

Table 7 Comparison with the state-of-the-art methods

Ref	Number of images	Database Used	Backbone Used	Covid-19 acc.
Proposed	103468	PADCHEST BIMCV-COVID19+ COVID-19 Radiography Chest X-ray	InceptionV3	0.97
[8]	2800	Chest X-ray	OptCoNet	0.98
[30]	1125	Chest X-ray	DarkCovidNet	0.98
[31]	196	Chest X-ray JSRT	VGG16	0.93
[7]	1428	Chest X-ray Covid-19 X-ray Pneumonia X-ray	MobileNetV2	0.98
[32]	502	Chest X-ray CoronaHack NLM JSRT	DenseNet103	0.92
[33]	2905	COVID-19 Radiography	A novel CNN	0.89
[15]	6432	Chest X-ray	ResNet-50	1
[15]	2905	COVID-19 Radiography	ResNet-50	1

Coefficient (MCC) [29] since the dataset is imbalanced. The model gets MCC as 0.6745 and 0.6541 for 2-class and 5-class, respectively.

Finally, our best results are obtained by using InceptionV3 as our backbone with no filtering applied. We obtained 84.57% test accuracy for the 2-class label merge and 81.03% test accuracy for the 5-class label merge. Notably, we obtained 97.03% test accuracy on predicting COVID diagnosed X-ray images in our 5-class dataset. Also, we obtained "normal", i.e. healthy class prediction accuracy of 93.20% with 5-class and 78.33% with 2-class.

We compare our results with the state-of-the-art methods in Table 7. Our method with 97.03% accuracy on the COVID images is one of the best performing methods for COVID detection. It is important to notice that the datasets for the other methods have at most 6,432 images. This sample count is very low compared to our 103,468 images. Our dataset, although splitted to 5 classes, has cases from 20 different diseases, which is much higher compared to the-state-of-the-art studies. Certainly, this variety and size adds additional value to our results as our method results with a better generalization. We should note down that the generalization problem is one of the main reasons why such methods have not been trusted for COVID detection in practice. COVID detection is of utmost importance; therefore, COVID accuracy is the main metric for our study. And, our method produces very good results for that while improving the generalization capabilities.

Additionally, we show the training accuracies for our method in Tables 8 and 9 for each class merge separately. We can see that in both cases, there is only a small difference between the training and test accuracies that tells us overfitting or underfitting is not a priority in our training. However, there are some low accuracies for some classes, i.e. "others" in 5-class merge. This can be explained by the mixed data samples in "others" class which makes characterization of this class harder than others.

Table 8 Training and validation accuracy between 2 classes Normal (0) and Abnormal class (1)

	Precision	Recall	f1-score	Support
Normal	0.82	0.78	0.80	10,029
Abnormal	0.86	0.89	0.87	15,531
Accuracy			0.85	25,560
Macro avg	0.84	0.83	0.84	25,560
Weighted avg	0.84	0.85	0.85	25,560

Table 9 Training and validation accuracy between 5 classes

	Precision	Recall	f1-score	Support
COPD Signs	0.68	0.63	0.66	5830
Covid	0.94	0.97	0.96	843
Normal	0.84	0.93	0.89	15,629
Others	0.58	0.34	0.43	1308
Pneumonia	0.92	0.64	0.76	2223
Accuracy			0.81	25,833
Macro avg	0.78	0.70	0.74	25,833
Weighted avg	0.80	0.81	0.80	25,833

5 Conclusion

One of the most used techniques for diagnosing certain diseases is assessing pathological chest X-rays. However, this task is yet to be fully automated, while such an automation would save hours of medical professionals. In the previous research, CNNs and similar structures are proposed as a method to automatically differentiate between the normal and diseased X-ray chest images. However, one of the lacking point of previous research was relatively small dataset, i.e. low sample size, bias between classes, low generalization, etc.

In order to address such issues, we evaluated how well deep CNNs perform on pathological chest X-ray classification using largest number of images, i.e. 103,468 images. We experimented with different class splits and different methods to finally obtain 84.57% accuracy for classifying between normal and diseased images. Moreover, we obtained 81.03% accuracy for classifying between 5 classes, i.e. COPD signs, COVID, Pneumonia, normal and others. Our method acquired 97.03% accuracy for COVID class which is significant if the method is used for COVID detection.

One of the shortcomings of our method is that, "others" class in the 5-class split includes images from many diseases. This makes the class hard to characterize, therefore causing a decrease in the performance. A further study can be done with an improvement of the data in this class. Alternatively, the network can be improved so that it learns low-performing classes better.

References

1. Zhu, N., Zhang, D., Wang, W., Li, X., Yang, B., Song, J., Zhao, X., Huang, B., Shi, W., Lu, R., et al.: A novel coronavirus from patients with pneumonia in china, 2019. New Engl. J. Med. (2020)
2. Zu, Z.Y., Jiang, M.D., Xu, P.P., Chen, W., Ni, Q.Q., Lu, G.M., Zhang, L.J.: Coronavirus disease 2019 (Covid-19): a perspective from china. Radiology **296**(2), E15–E25 (2020)
3. Chan, J.F.-W., Yuan, S., Kok, K.-H., To, K.K.-W., Chu, H., Yang, J., Xing, F., Liu, J., Yip, C.C.-Y., Poon, R.W.-S., et al.: A familial cluster of pneumonia associated with the 2019 novel coronavirus indicating person-to-person transmission: a study of a family cluster. Lancet **395**(10223), 514–523 (2020)
4. Zhao, W., Zhong, Z., Xie, X., Yu, Q., Liu, J.: Relation between chest ct findings and clinical conditions of coronavirus disease (Covid-19) pneumonia: a multicenter study. Am. J. Roentgenol. **214**(5), 1072–1077 (2020)
5. Hemdan, E.E.D., Shouman, M.A., Karar, M.E.: Covidx-net: a framework of deep learning classifiers to diagnose Covid-19 in X-ray images. arXiv preprint arXiv:2003.11055 (2020)
6. Linda, W.: A tailored deep convolutional neural network design for detection of Covid-19 cases from chest radiography images. J. Netw. Comput. Appl. **20**, 1–12 (2020)
7. Apostolopoulos, I.D., Mpesiana, T.A.: Covid-19: automatic detection from X-ray images utilizing transfer learning with convolutional neural networks. Phys. Eng. Sci. Med. **43**(2), 635–640 (2020)
8. Goel, T., Murugan, R., Mirjalili, S., Chakrabartty, D.K.: Optconet: an optimized convolutional neural network for an automatic diagnosis of COVID-19. Appl. Intell. **51**(3), 1351–1366 (2021). https://doi.org/10.1007/s10489-020-01904-z
9. Apostolopoulos, I.D., Aznaouridis, S.I., Tzani, M.A.: Extracting possibly representative Covid-19 biomarkers from x-ray images with deep learning approach and image data related to pulmonary diseases. J. Med. Biol. Eng. **40**, 462–469 (2020)
10. Vinodkumar, P.K., Ozcinar, C., Anbarjafari, G.: Prediction of SGRNA off-target activity in crispr/cas9 gene editing using graph convolution network. Entropy **23**(5), 608 (2021)
11. Elshatoury, H., Cruciani, F., Zumerle, F., Storti, S.F., Altmann, A., Lorenzi, M., Anbarjafari, G., Menegaz, G., Galazzo, I.B.: Disentangling the association between genetics and functional connectivity in mild cognitive impairment. In: 2021 IEEE EMBS International Conference on Biomedical and Health Informatics (BHI), pp. 1–4. IEEE (2021)
12. Avots, E., Jermakovs, K., Bachmann, M., Päeske, L., Ozcinar, C., Anbarjafari, G.: Ensemble approach for detection of depression using EEG features. Entropy **24**(2), 211 (2022)
13. Narin, A., Kaya, C., Pamuk, Z.: Automatic detection of coronavirus disease (Covid-19) using X-ray images and deep convolutional neural networks. Pattern Anal. Appl. (2021). https://doi.org/10.1007/s10044-021-00984-y
14. Minaee, S., Kafieh, R., Sonka, M., Yazdani, S., Jamalipour Soufi, G.: Deep-covid: Predicting covid-19 from chest X-ray images using deep transfer learning. Med. Image Anal. **65**, 101794 (2020)
15. Pathan, S., Siddalingaswamy, P., Ali, T.: Automated detection of covid-19 from chest X-ray scans using an optimized CNN architecture. Appl. Soft Comput. **104**, 107238 (2021)
16. Bustos, A., Pertusa, A., Salinas, J.-M., de la Iglesia-Vayá, M.: Padchest: a large chest X-ray image dataset with multi-label annotated reports. Med. Image Anal. **66**, 101797 (2020)
17. Vayá, M.d. l.I., Saborit, J.M., Montell, J.A., Pertusa, A., Bustos, A., Cazorla, M., Galant, J., Barber, X., Orozco-Beltrán, D., García-García, F. et al.: Bimcv covid-19+: a large annotated dataset of rx and ct images from covid-19 patients. arXiv preprint arXiv:2006.01174 (2020)
18. Chowdhury, M.E., Rahman, T., Khandakar, A., Mazhar, R., Kadir, M.A., Mahbub, Z.B., Islam, K.R., Khan, M.S., Iqbal, A.: Can ai help in screening viral and covid-19 pneumonia? IEEE Access **8**, 132 665-132 676 (2020)
19. Rahman, T., Khandakar, A., Qiblawey, Y., Tahir, A., Kiranyaz, S., Kashem, S.B.A., Islam, M.T., Al Maadeed, S., Zughaier, S.M., Khan, M.S., et al.: Exploring the effect of image enhancement techniques on covid-19 detection using chest X-ray images. Comput. Biol. Med. **132**, 104319 (2021)
20. Parveen, N., Sathik, M.M.: Detection of pneumonia in chest X-ray images. J. X-ray Sci. Technol. **19**(4), 423–428 (2011)
21. Vecvanags, A., Aktas, K., Pavlovs, I., Avots, E., Filipovs, J., Brauns, A., Done, G., Jakovels, D., Anbarjafari, G.: Ungulate detection and species classification from camera trap images using retinanet and faster R-CNN. Entropy **24**(3), 353 (2022)
22. Kamińska, D., Aktas, K., Rizhinashvili, D., Kuklyanov, D., Sham, A.H., Escalera, S., Nasrollahi, K., Moeslund, T.B., Anbarjafari, G.: Two-stage recognition and beyond for compound facial emotion recognition. Electronics **10**(22), 2847 (2021)
23. Aktas, K., Demirel, M., Moor, M., Olesk, J., Ozcinar, C., Anbarjafari, G.: Spatiotemporal based table tennis stroke-type assessment. SIViP **15**(7), 1593–1600 (2021)
24. Szegedy, C., Vanhoucke, V., Ioffe, S., Shlens, J., Wojna, Z.: Rethinking the inception architecture for computer vision. CoRR, vol. abs/1512.00567 (2015). Available: http://arxiv.org/abs/1512.00567
25. Ioffe, S., Szegedy, C.: Batch normalization: accelerating deep network training by reducing internal covariate shift. arXiv preprint arXiv:1502.03167 (2015)
26. Simonyan, K.,Zisserman, A.: Very deep convolutional networks for large-scale image recognition. arXiv preprint arXiv:1409.1556 (2014)
27. He, K., Zhang, X., Ren, S., Sun, J.: Deep residual learning for image recognition. CoRR, vol. abs/1512.03385 (2015) [Online]. Available: http://arxiv.org/abs/1512.03385
28. Zoph, B., Vasudevan, V., Shlens, J., Le, Q.V.: Learning transferable architectures for scalable image recognition. CoRR, vol. abs/1707.07012 (2017) [Online]. Available: http://arxiv.org/abs/1707.07012
29. Matthews, B.W.: Comparison of the predicted and observed secondary structure of t4 phage lysozyme. Biochimica et Biophysica Acta (BBA)-Protein Struct. **405**(2), 442–451 (1975)

30. Ozturk, T., Talo, M., Yildirim, E.A., Baloglu, U.B., Yildirim, O., Acharya, U.R.: Automated detection of Covid-19 cases using deep neural networks with X-ray images. Comput. Biol. Med. **121**, 103792 (2020)
31. Abbas, M.G.A., Abdelsamea, M.M.: Classification of covid-19 in chest X-ray images using detrac deep convolutional neural network (2020). arXiv preprint arXiv:2003.13815
32. Oh, Y., Park, S., Ye, J.C.: Deep learning Covid-19 features on CXR using limited training data sets. IEEE Trans. Med. Imaging **39**(8), 2688–2700 (2020)
33. Nour, M., Cömert, Z., Polat, K.: A novel medical diagnosis model for Covid-19 infection detection based on deep features and bayesian optimization. Appl. Soft Comput. **97**, 106580 (2020)